Full Rank Hypothesis (FRH) Study

Camilla Polvara

1 Introduction

The Full Rank Hypothesis (FRH) is a framework for analyzing the structure and dynamics of quantum many-body wavefunctions. In this study, we investigate the validity and implications of the FRH across several models, including the one-dimensional transverse field Ising model (TFIM), the PXP model, and the TFIM defined on an icosahedral geometry. Our primary focus is to explore the relationship between the FRH and the presence of quantum scar states, which are known to deviate from typical thermalization behavior and exhibit atypically low entanglement compared to other eigenstates at similar energies. Notably, in some of these models, the reduced density matrix (RDM) of a subsystem of n spins - where $n < N/2$ and N is the full system size - fails to have full rank, indicating a breakdown of the FRH.

2 1D Transverse Field Ising Model (TFIM)

The transverse field Ising model is one of the simplest paradigms for quantum phase transitions. The Hamiltonian is given by:

$$H = -J \sum_{i=1}^{N} \sigma_i^x \sigma_{i+1}^x - h \sum_{i=1}^{N} \sigma_i^z, \tag{1}$$

where J is the interaction strength, h is the transverse field and N is the number of sites. σ^x, σ^z are the (x, z) Pauli matrices:

$$\sigma_x = \begin{pmatrix} 0 & 1 \\ 1 & 0 \end{pmatrix}, \quad \sigma_y = \begin{pmatrix} 0 & -i \\ i & 0 \end{pmatrix}, \quad \sigma_z = \begin{pmatrix} 1 & 0 \\ 0 & -1 \end{pmatrix} \tag{2}$$

The Pauli raising and lowering operators, which we will need shortly, are defined in terms of the Pauli matrices σ^x and σ^y as follows:

$$\sigma^{\pm} = \frac{1}{2}(\sigma_x \pm i\sigma_y), \quad \sigma^+ = \begin{pmatrix} 0 & 1 \\ 0 & 0 \end{pmatrix}, \quad \sigma^- = \begin{pmatrix} 0 & 0 \\ 1 & 0 \end{pmatrix} \tag{3}$$

All the matrices are defined at site i, meaning that

$$\sigma_i = \mathbb{I}_2 \otimes \ldots \otimes \underbrace{\sigma}_{i} \otimes \ldots \otimes \mathbb{I}_2 \tag{4}$$

$$\sigma_i \sigma_j = \mathbb{I}_2 \otimes \ldots \otimes \underbrace{\sigma}_{i} \otimes \ldots \otimes \underbrace{\sigma}_{j} \otimes \ldots \otimes \mathbb{I}_2 \tag{5}$$

The TFIM Hamiltonian exhibits the following symmetries:

- $\mathbb{Z}_2$ **symmetry (Global Spin Flip):** The Hamiltonian is invariant under a global spin flip along the x-axis:
$$\sigma_i^x \to -\sigma_i^x, \quad \sigma_i^z \to \sigma_i^z$$

- **Time-Reversal Symmetry:** Since the Hamiltonian contains only real terms, it is invariant under time-reversal symmetry $\mathcal{T}$, which acts as:
$$\mathcal{T} : i \to -i, \quad \sigma_i^x, \sigma_i^z \to \sigma_i^x, \sigma_i^z$$

- **Translational Symmetry:** With periodic boundary conditions, the model is invariant under discrete lattice translations:
$$i \to i + 1$$

- **Reflection (Parity) Symmetry:** For chains with reflection-symmetric boundaries, the model is invariant under spatial inversion:
$$i \to N - i + 1$$

The FRH in this system is investigated by analyzing the eigenstates and their rank structure $(3, 4$-spins rdms) in different parameter regimes. In the case considered, $J = h = 1$ (critical regime).

To diagonalize the transverse field Ising model (TFIM), we start from the Hamiltonian Eq. (1) with periodic boundary conditions ($\sigma_{N+1} = \sigma_1$).

The first step is to map spins to fermions using the Jordan-Wigner transformation:

$$\sigma_i^- = F_i c_i \quad \sigma_i^+ = F_i c_i^\dagger \quad \sigma_i^z = 2c_i^\dagger c_i - 1 \tag{6}$$

where c_j are canonical fermionic annihilation operators satisfying

$$\{c_i, c_j^\dagger\} = \{c_i^\dagger, c_j\} = \delta_{i,j}, \quad \{c_i^\dagger, c_j^\dagger\} = \{c_i, c_j\} = 0 \tag{7}$$

and we have defined the Jordan-Wigner string operator,

$$F_i = (-1)^{n_i} = e^{i\pi \sum_{l=1}^{i-1} c_l^\dagger c_l} = \prod_{l=1}^{i-1} (1 - 2c_l^\dagger c_l) \tag{8}$$

which is crucial for ensuring the correct fermionic anticommutation relations when mapping spin operators to fermionic operators. F_i introduces a non-local phase that keeps track of how many fermions are to the left of site i, enforcing the correct sign changes due to fermionic statistics.

The following properties hold

$$F_i c_i = c_i F_i, \quad F_i c_i^\dagger = c_i^\dagger F_i \tag{9}$$

$$F_i F_{i+1} = (-1)^{c_i^\dagger c_i} = (-1)^{n_i} \tag{10}$$

$$\left(c_i^\dagger + c_i\right)(-1)^{n_i} = c_i^\dagger - c_i \tag{11}$$

With the application of the Jordan-Wigner mapping, the two terms in Eq. (1) become

$$\sigma_i^x \sigma_{i+1}^x = F_i \left(c_i^\dagger + c_i\right) F_{i+1} \left(c_{i+1}^\dagger + c_{i+1}\right) \tag{12}$$

$$= \left(c_i^\dagger + c_i\right) F_i F_{i+1} \left(c_{i+1}^\dagger + c_{i+1}\right) \tag{13}$$

$$= \left(c_i^\dagger + c_i\right)(-1)^{n_i} \left(c_{i+1}^\dagger + c_{i+1}\right) \tag{14}$$

$$= \left(c_i^\dagger - c_i\right) \left(c_{i+1}^\dagger + c_{i+1}\right) \tag{15}$$

and

$$\sigma_i^z = 2c_i^\dagger c_i - 1 \tag{16}$$

so that the TFIM Hamiltonian becomes quadratic in fermions:

$$H = -J \sum_{i=1}^{N} \left(c_i^\dagger c_{i+1} + c_{i+1}^\dagger c_i + c_i^\dagger c_{i+1}^\dagger + c_{i+1} c_i - 2h c_i^\dagger c_i + h\right) \tag{17}$$

We then Fourier transform:

$$c_j = \frac{1}{\sqrt{N}} \sum_k e^{ikaj} c_k, \qquad k = \frac{2\pi}{Na}\left(n + \frac{1}{2}\right), \quad n \in \mathbb{Z} \tag{18}$$

where a is the spacing between lattice sites (we set $a = 1$), to obtain the momentum-space Hamiltonian:

$$H = -J \sum_k \left[(\cos k - h)(c_k^\dagger c_k - c_{-k} c_{-k}^\dagger) + i \sin k (c_k^\dagger c_{-k}^\dagger + c_k c_{-k}) + h \right] \tag{19}$$

This Hamiltonian can be diagonalized by a Bogoliubov transformation:

$$\gamma_k = u_k c_k + v_k c_{-k}^\dagger, \quad \gamma_k^\dagger = u_k^* c_k^\dagger + v_k^* c_{-k} \tag{20}$$

with coefficients $u_k, v_k \in \mathbb{C}$, such that $|u_k|^2 + |v_k|^2 = 1$ and such that the transformed Hamiltonian becomes:

$$H = \sum_k \varepsilon_k \left(\gamma_k^\dagger \gamma_k - \frac{1}{2} \right) \tag{21}$$

where the quasiparticle dispersion relation is

$$\varepsilon_k = 2J \sqrt{(\cos k - h)^2 + \sin k^2} = 2J \sqrt{1 + h^2 - 2h \cos k} \tag{22}$$

It's possible to show that the correct u_k, v_k leading to this dispersion are:

$$u_k = \cos \frac{\theta_k}{2}, \quad v_k = \sin \frac{\theta_k}{2}, \quad \tan \theta_k = \frac{\sin k}{h - \cos k} \tag{23}$$

The operators γ_k describe non-interacting fermionic quasiparticles:

$$\{\gamma_k, \gamma_p^\dagger\} = \{\gamma_k^\dagger, \gamma_p\} = \delta_{k,p}, \quad \{\gamma_k^\dagger, \gamma_p^\dagger\} = \{\gamma_k, \gamma_p\} = 0 \tag{24}$$

and the number operators

$$n_k = \gamma_k^\dagger \gamma_k \tag{25}$$

are conserved quantities, since they commute with the Hamiltonian:

$$[H, n_k] = 0 \quad \forall k \tag{26}$$

This yields an infinite set of conserved charges, one for each allowed momentum k. These charges completely specify each eigenstate. However, these occupation numbers n_k are nonlocal in real space. Let us show this explicitly.

$$n_k = \gamma_k^\dagger \gamma_k = \left(u_k^* c_k^\dagger + v_k^* c_{-k} \right) \left(u_k c_k + v_k c_{-k}^\dagger \right) \tag{27}$$

$$= |u_k|^2 c_k^\dagger c_k + u_k^* v_k c_k^\dagger c_{-k}^\dagger + u_k v_k^* c_{-k} c_k + |v_k|^2 c_{-k} c_{-k}^\dagger \tag{28}$$

We can express each term in Eq. (27) in real space. The inverse Fourier transform is:

$$c_k = \frac{1}{\sqrt{N}} \sum_{j=1}^N e^{ikj} c_j \tag{29}$$

For example, the first term becomes

$$c_k^\dagger c_k = \frac{1}{N} \sum_{j,j'=1}^N e^{ik(j-j')} c_j^\dagger c_{j'} \tag{30}$$

We now go back to Pauli matrices by applying the inverse Jordan-Wigner transformation

$$c_j = \frac{1}{2} \left(\prod_{l=1}^{j-1} \sigma_l^z \right) \sigma_j^- \tag{31}$$

so that

$$c_k^\dagger c_k = \frac{1}{16N} \sum_{j,j'=1}^{N} e^{ik(j-j')} \left(\prod_{l=1}^{j-1} \sigma_l^z\right) \left(\sigma_j^x + i\sigma_j^y\right) \left(\prod_{l'=1}^{j'-1} \sigma_{l'}^z\right) \left(\sigma_{j'}^x - i\sigma_{j'}^y\right) \tag{32}$$

We split the calculation into 3 parts, $j = j'$, and $j \neq j'$ ($j < j'$, $j > j'$). The commutation relations of the Pauli matrices will come in handy:

$$[\sigma_\alpha^i, \sigma_\beta^j] = 2i\epsilon_{ijk}\sigma_\alpha^k \,\delta_{\alpha,\beta}, \quad i,j,k = x,y,z \tag{33}$$

- $j = j'$

$$\left(\prod_{l=1}^{j-1} \sigma_l^z\right) \left(\sigma_j^x + i\sigma_j^y\right) \left(\prod_{l'=1}^{j'-1} \sigma_{l'}^z\right) \left(\sigma_{j'}^x - i\sigma_{j'}^y\right) = \left(\prod_{l=1}^{j-1} (\sigma_l^z)^2\right) \left(\sigma_j^x + i\sigma_j^y\right) \left(\sigma_j^x - i\sigma_j^y\right) \tag{34}$$

$$= \left(\sigma_j^x + i\sigma_j^y\right) \left(\sigma_j^x - i\sigma_j^y\right) = \left(\sigma_j^x\right)^2 + \left(\sigma_j^y\right)^2 - i[\sigma_j^x, \sigma_j^y] = 2\left(\mathbb{I}_2 + \sigma_j^z\right) \tag{35}$$

- $j < j'$

$$\prod_{l'=1}^{j'-1} \sigma_{l'}^z = \left(\prod_{l'=1}^{j-1} \sigma_{l'}^z\right) \left(\prod_{l''=j}^{j'-1} \sigma_{l''}^z\right) \tag{36}$$

So that

$$\left(\prod_{l=1}^{j-1} \sigma_l^z\right) \left(\sigma_j^x + i\sigma_j^y\right) \left(\prod_{l'=1}^{j'-1} \sigma_{l'}^z\right) \left(\sigma_{j'}^x - i\sigma_{j'}^y\right) \tag{37}$$

$$= \left(\prod_{l=1}^{j-1} \sigma_l^z\right)^2 \left(\sigma_j^x + i\sigma_j^y\right) \left(\prod_{l'=j}^{j'-1} \sigma_{l'}^z\right) \left(\sigma_{j'}^x - i\sigma_{j'}^y\right) \tag{38}$$

$$= \left(\sigma_j^x + i\sigma_j^y\right) \left(\prod_{l'=j}^{j'-1} \sigma_{l'}^z\right) \left(\sigma_{j'}^x - i\sigma_{j'}^y\right) \tag{39}$$

$$= \left(\sigma_j^x + i\sigma_j^y\right) \sigma_j^z \left(\prod_{l'=j+1}^{j'-1} \sigma_{l'}^z\right) \left(\sigma_{j'}^x - i\sigma_{j'}^y\right) \tag{40}$$

$$= \left[\left(\sigma_j^z - 2\mathbb{I}_2\right)\left(\sigma_j^x + i\sigma_j^y\right)\right] \left(\prod_{l'=j+1}^{j'-1} \sigma_{l'}^z\right) \left(\sigma_{j'}^x - i\sigma_{j'}^y\right) \tag{41}$$

$$= \left(\sigma_j^z - 2\mathbb{I}_2\right) \left(\prod_{l=j+1}^{j'-1} \sigma_l^z\right) \left(\sigma_j^x + i\sigma_j^y\right) \left(\sigma_{j'}^x - i\sigma_{j'}^y\right) \tag{42}$$

- $j > j'$

$$\prod_{l=1}^{j-1} \sigma_l^z = \left(\prod_{l=1}^{j'-1} \sigma_l^z\right) \left(\prod_{l'=j'}^{j-1} \sigma_{l'}^z\right) \tag{43}$$

Then, proceeding as before

4

$$\left(\prod_{l=1}^{j-1} \sigma_l^z\right)(\sigma_j^x + i\sigma_j^y)\left(\prod_{l'=1}^{j'-1} \sigma_{l'}^z\right)\left(\sigma_{j'}^x - i\sigma_{j'}^y\right) \tag{44}$$

$$= \left(\prod_{l=1}^{j'-1} \sigma_l^z\right)^2 \left(\prod_{l'=j'}^{j-1} \sigma_{l'}^z\right)(\sigma_j^x + i\sigma_j^y)\left(\sigma_{j'}^x - i\sigma_{j'}^y\right) \tag{45}$$

$$= \left(\prod_{l'=j'}^{j-1} \sigma_{l'}^z\right)(\sigma_j^x + i\sigma_j^y)\left(\sigma_{j'}^x - i\sigma_{j'}^y\right) \tag{46}$$

Putting everything together

$$c_k^\dagger c_k = \frac{1}{16N} \sum_{j,j'=1}^{N} e^{ik(j-j')} \Gamma_{jj'} \tag{47}$$

where the operator-valued kernel $\Gamma_{jj'}$ depends on the relative positions of j and j' as follows:

$$\Gamma_{jj'} = \begin{cases} 2(\mathbb{I}_2 + \sigma_j^z), & \text{if } j = j' \\[2ex] (\sigma_j^z - 2\mathbb{I}_2)\left(\prod_{l=j+1}^{j'-1} \sigma_l^z\right)(\sigma_j^x + i\sigma_j^y)(\sigma_{j'}^x - i\sigma_{j'}^y), & \text{if } j < j' \\[2ex] \left(\prod_{l=j'}^{j-1} \sigma_l^z\right)(\sigma_j^x + i\sigma_j^y)(\sigma_{j'}^x - i\sigma_{j'}^y), & \text{if } j > j' \end{cases} \tag{48}$$

Analogous expressions hold for the other terms of Eq. (32). The most important point is that the sum for all of them runs over the whole lattice (ie. up to N), and is therefore not local. In other words, there do not exist locally commuting charges in the TFIM; the occupation numbers n_k commute with the TFIM Hamiltonian but they are defined globally. This is confirmed by numerical analysis too. In the critical regime, the 3/4 spins rdms of the 12 spins TFIM are full rank:
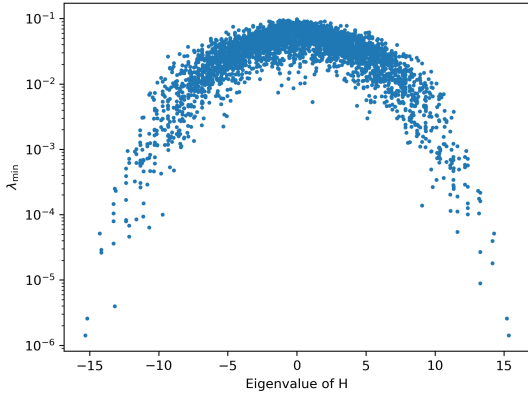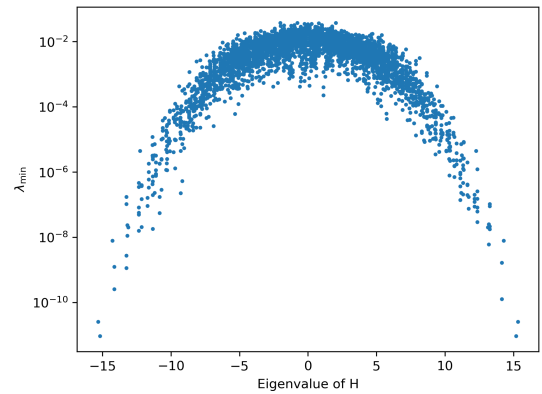

Figure 1: Minimum eigenvalue for 3-spins rdm

Figure 2: Minimum eigenvalue of 4-spins rdm

In other words, the FRH is generically satisfied.
mention majorana fermions notation. TFIM with obc has scars!

3 PXP Model

The PXP model describes constrained dynamics relevant to Rydberg atom arrays. We will consider the simpler case of an array of spins, i.e. of $0, 1$. The Hamiltonian takes the form (the tensor product between the operators at different sites, including $\mathbb{I}_2$ is left implicit):

$$H = \sum_{i=1}^{N} P_{i-1}\sigma_i^x P_{i+1}, \tag{49}$$

where, using the convention $|0\rangle = \begin{pmatrix} 1 \\ 0 \end{pmatrix}, |1\rangle = \begin{pmatrix} 0 \\ 1 \end{pmatrix}$

$$\sigma^x = |0\rangle\langle 1| + |1\rangle\langle 0| = \begin{pmatrix} 0 & 1 \\ 1 & 0 \end{pmatrix} \tag{50}$$

$$P = \frac{1}{2}(\mathbb{I}_2 + \sigma^z) = |0\rangle\langle 0| = \begin{pmatrix} 1 & 0 \\ 0 & 0 \end{pmatrix} \tag{51}$$

The projector P_i ensures that adjacent excitations $|\ldots 11\ldots\rangle$ are forbidden. By definition, the PXP model is defined only for the states without adjacent excitations, and the presence of the projectors P just make sure the Hamiltonian remains in this subspace. We call the subspace of states allowed by the PXP model *PXP subspace*, whereas the kinetic constraint on the Hilbert space is known as *Rydberg blockade*.

Eq. (49) admits open or periodic boundary conditions (obc, pbc). For the former, we set $P_0 = P_{N+1} = \mathbb{I}_2$, and for the latter $P_0 = P_N, P_{N+1} = P_1$.

For example, for $N = 3$, the PXP Hamiltonian with open and periodic boundary conditions is given by:

$$H_{\text{obc}} = \sigma_1^x P_2 + P_1\sigma_2^x P_3 + P_2\sigma_3^x, \tag{52}$$
$$H_{\text{pbc}} = \sigma_1^x P_2 P_3 + P_1\sigma_2^x P_3 + P_1 P_2\sigma_3^x. \tag{53}$$

The PXP subspace for obc is spanned by states $|0,0,0\rangle, |1,0,0\rangle, |0,1,0\rangle, |0,0,1\rangle, |1,0,1\rangle$, whereas for pbc it is spanned by $|0,0,0\rangle, |1,0,0\rangle, |0,1,0\rangle, |0,0,1\rangle$. The three-spin states that contain adjacent excitations—i.e., those that violate the Rydberg blockade constraint—are, for open boundary conditions: $|1,1,0\rangle, |0,1,1\rangle$, and $|1,1,1\rangle$. For periodic boundary conditions, the state $|1,0,1\rangle$ is also forbidden due to the wrap-around interaction between site 3 and site 1.

These states lie outside the PXP subspace. Nevertheless, one can formally act on them with the PXP Hamiltonian, and the result is zero: they are annihilated by the Hamiltonian.

It's easy to compute the dimension of the PXP subspace for a generic number of sites N, and to show that it's related to the Fibonacci sequence:

$$d_N^{\text{obc}} = F_{N+2}, \quad d_N^{\text{pbc}} = F_{N-1} + F_{N+1} \tag{54}$$

where F_N is the N-th Fibonacci number ($F_0 = 0, F_1 = 1, F_N = F_{N-1} + F_{N-2}$ for $N \geq 2$).
Going back to the $N = 3$ example, we have

$$d_3^{\text{obc}} = F_5 = 5, \tag{55}$$
$$d_3^{\text{pbc}} = F_2 + F_4 = 1 + 3 = 4, \tag{56}$$

as expected.

We have seen that the forbidden states are annihilated by the PXP Hamiltonian. In other words, applying the PXP Hamiltonian to either the PXP subspace or its complement does not allow transitions between them. This implies that the two sectors are dynamically disconnected. As a result, the Hilbert space undergoes fragmentation.

In the absence of the Rydberg blockade constraint, the model would be integrable in the sense that the dynamics could explore the full Hilbert space, and all states would thermalize. However, due to the kinetic constraint imposed by the blockade, certain states become dynamically isolated and cannot thermalize. This fragmentation of the Hilbert space leads to the emergence of nonthermal states, which are known as *quantum scars*.

Among the nonthermal states in the PXP model, a particularly striking example is the so-called Z_2 Néel state, defined as $|\mathbb{Z}_2\rangle = |1,0,1,0,\ldots\rangle$, along with its translated counterpart $|\mathbb{Z}_2'\rangle = |0,1,0,1,\ldots\rangle$.

These two states lie deep within the PXP subspace and exhibit atypical dynamics under the action of the Hamiltonian, characterized by long-lived oscillations and slow thermalization. This behavior has been associated with the presence of quantum many-body scars.

One way to understand the emergence of scars in the PXP model is through the construction of a *tower of states* built on top of the $|\mathbb{Z}_2\rangle$ and $|\mathbb{Z}'_2\rangle$ states. These towers consist of a set of special eigenstates that are approximately equally spaced in energy and have large overlap with initial product states such as $|\mathbb{Z}_2\rangle$. A useful analytical framework for constructing such towers is the *Forward Scattering Approximation* (FSA).

In the FSA, one begins with a reference state—typically $|\mathbb{Z}_2\rangle$—and iteratively applies the Hamiltonian, but only retains the part of the resulting state that is orthogonal to all previously generated states. This generates an approximately closed subspace, the FSA subspace, which captures the essence of the scarred eigenstates and reproduces many of their qualitative features, including their energy spacing and overlap structure.

Interestingly, there exists a related model in which the forward scattering approximation becomes *exact*: the so-called *free paramagnetic model*, defined by relaxing the Rydberg blockade constraint in a controlled way. This model can be viewed as a deformation of the PXP Hamiltonian in which the scar structure is lifted into an exact set of eigenstates. As such, it serves as a useful toy model for understanding the mechanisms that protect and stabilize scars in the constrained PXP dynamics.

The paramagnetic model is defined by the Hamiltonian

$$H_{\mathrm{PM}} = \sum_{i=1}^{N} \sigma_i^x = H_+ + H_- \tag{57}$$

where H_+, H_- are called forward and backward propagator, and they are defined as

$$H_+ = \sum_{j \in \mathrm{odd}} \sigma_j^- + \sum_{j \in \mathrm{even}} \sigma_j^+ \tag{58}$$

$$H_- = \sum_{j \in \mathrm{odd}} \sigma_j^+ + \sum_{j \in \mathrm{even}} \sigma_j^- \tag{59}$$

The Hamiltonian H_{PM} acts globally on all spins without any constraints. The key insight is that, when restricted to the subspace generated by the repeated action of H_+ on the Néel state $|\mathbb{Z}_2\rangle = |1, 0, 1, 0, \dots\rangle$, the dynamics becomes exactly solvable and exhibits a hidden SU(2) algebraic structure.

Define an effective SU(2) ladder as follows:

$$N_{k+1}|k+1\rangle = H_+|k\rangle, \quad \text{for } k = 0, 1, \dots, N, \tag{60}$$

where N_{k+1} is the normalization constant for the state $|k+1\rangle$, and for a generic k it's iteratively defined as

$$N_k = \sqrt{k\,(N - k + 1)} \tag{61}$$

The tower starts with the state $|0\rangle = |\mathbb{Z}_2\rangle$ and ends with the translated Néel state $|\mathbb{Z}'_2\rangle$:

$$|\mathbb{Z}'_2\rangle = |N\rangle = \frac{(H_+)^N}{\sqrt{N}}|\mathbb{Z}_2\rangle \tag{62}$$

The states $\{|k\rangle\}$ span a finite-dimensional Krylov subspace generated by repeated applications of the forward scattering operator H_+ on the Néel state $|\mathbb{Z}_2\rangle$. In the paramagnetic model, this Krylov subspace is invariant under the action of the Hamiltonian $H_{\mathrm{PM}} = H_+ + H_-$, and forms an exact irreducible representation of SU(2).

Within this subspace, the states $|k\rangle$ form an exact tower of eigenstates of the Casimir operator of the SU(2) structure, defined as

$$H^2 = \frac{1}{2}\{H_+, H_-\} + \frac{1}{4}(H_z)^2 \tag{63}$$

where

$$H_z = \sum_j \left(\sigma^z_{2j} - \sigma^z_{2j+1} \right) \tag{64}$$

The forward and backward propagators generate transitions within the tower of states:

$$H_+ |k\rangle \propto |k+1\rangle, \quad H_- |k\rangle \propto |k-1\rangle \tag{65}$$

and the commutation relations of the $SU(2)$ algebra hold

$$[H_+, H_-] = H_z \tag{66}$$

Also note that the Casimir operator H^2 commutes with the paramagnet Hamiltonian:

$$[H_{\text{PM}}, H^2] = 0, \tag{67}$$

reflecting the fact that H_{PM} preserves the $SU(2)$ representation structure. This algebraic structure leads to equally spaced energy levels and it provides a useful toy model for understanding quantum scars in the PXP model.

In the PXP model, the kinetic constraint from the Rydberg blockade breaks the exact SU(2) structure. However, one can still construct an approximate tower of states using the *Forward Scattering Approximation* (FSA).
The forward and backward propagators are now defined as

$$H_+ = \sum_{j \,\in\, \text{odd}} P_{j-1} \sigma^-_j P_{j+1} + \sum_{j \,\in\, \text{even}} P_{j-1} \sigma^+_j P_{j+1} \tag{68}$$

$$H_- = \sum_{j \,\in\, \text{odd}} P_{j-1} \sigma^+_j P_{j+1} + \sum_{j \,\in\, \text{even}} P_{j-1} \sigma^-_j P_{j+1} \tag{69}$$

To construct the FSA tower in the PXP model, one starts again from the Néel state $|\mathbb{Z}_2\rangle$, and recursively generates a set of orthogonal states $\{|k\rangle\}$ as follows:

$$|0\rangle = |\mathbb{Z}_2\rangle, \tag{70}$$

$$|1\rangle = H_+ |0\rangle, \tag{71}$$

$$N_{k+1} |k+1\rangle = (H - a_k) |k\rangle - N_k |k-1\rangle, \tag{72}$$

where the coefficient $a_k = \langle H\, k|k\rangle$ is chosen to enforce orthogonality between states $|k+1\rangle$ and $|k\rangle$ (not necessary in the paramagnet, where the SU(2) structure is exact and the basis vectors remain orthogonal by construction). Eq. (72) is the PXP-modified version of Eq. (60), since for the PXP model, $H_+ |k\rangle \not\propto |k+1\rangle$. Both forward and backward propagators $H_\pm$ are needed to generate the FSA states in the PXP model (not just H_+).
Unlike in the paramagnetic model, the action of H_+ on $|k\rangle$ does not remain entirely within the Krylov subspace span$\{|0\rangle, \ldots, |N\rangle\}$. This reflects the fact that the SU(2) ladder structure is only approximate, and that H_+, H_-, and $H_z = [H_+, H_-]$ no longer satisfy the exact SU(2) commutation relations.
The non-closure of the FSA basis can be quantified by evaluating the norm of the residual vector

$$|\delta_k\rangle = H_- |k-1\rangle - N_{k-1} |k-2\rangle, \tag{73}$$

which is exactly zero in the paramagnetic model but nonzero in the PXP model. This deviation leads to slight distortions in the energy spectrum of the approximate tower, as well as to reduced orthogonality between the FSA states.

Nevertheless, the FSA remains remarkably effective in capturing the essential features of the scarred eigenstates of the PXP model. These special eigenstates have large overlap with the FSA basis, exhibit near-equal energy spacing, and support long-lived coherent oscillations when the system is initialized in $|\mathbb{Z}_2\rangle$.

We numerically analyzed the PXP model for a chain of 12 spins with periodic boundary conditions (PBC), aiming to characterize quantum scarred eigenstates through three main diagnostics: their overlap
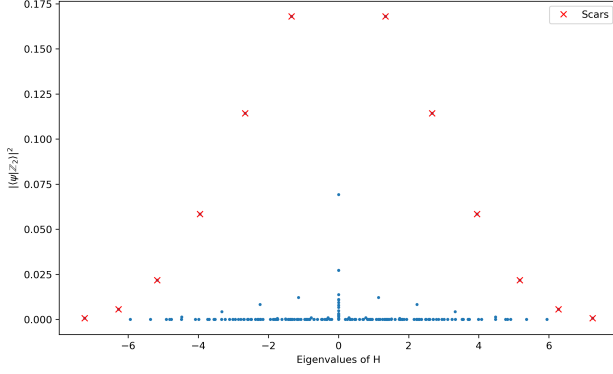
Figure 3: Overlap between eigenstates and the Néel $\mathbb{Z}_2$ state. Quantum scars exhibit stronger overlap, in contrast to thermal states.
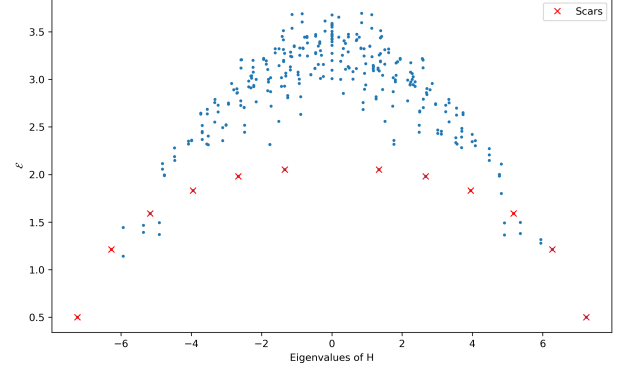

Figure 4: Bipartite entanglement entropy of eigenstates. Scars exhibit low entanglement relative to thermal states.

with the Néel $\mathbb{Z}_2$ state, their bipartite entanglement entropy, and, most importantly, the properties of their reduced density matrices (RDMs) for three adjacent spins.

To probe the local structure of scarred eigenstates, we examined the RDM of the spins $[5, 6, 7]$ (equivalent results were observed for all triplets of adjacent spins, as expected from translation invariance). For each eigenstate, we computed the rank of the 3-spin RDM. The results are reported in the table below.

We found that all 3-spin RDMs associated with scarred eigenstates have **rank 5** (not full rank, 8), and consistently contain **three zero rows and columns**, corresponding to the **forbidden states** $|011\rangle, |110\rangle, |111\rangle$. These are precisely the configurations excluded by the Rydberg blockade constraint. This pattern highlights the failure of FRH in the PXP model not because of emergent symmetries or conserved quantities (such as the hidden SU(2) symmetry, present in the free paramagnetic model but not in the PXP model), but because of the nonthermal constraints encoded directly at the level of local Hilbert space structure. The Rydberg blockade enforces a projection onto a kinetically constrained subspace, carving out a rigid structure that persists even in reduced local descriptions of the system.

mention allowed null states. you can see these degenerate states in fig 3 with neel overlap- vertical tower.

4 TFIM on Icosahedron

The transverse field Ising model (TFIM) can be studied on the icosahedral lattice, where the geometry introduces frustration even in the absence of disorder. The Hamiltonian takes the standard form

$$H = -J \sum_{\langle i,j \rangle} \sigma_i^x \sigma_j^x - h \sum_i \sigma_i^z, \tag{74}$$

When the TFIM is defined on the icosahedron, the symmetry structure changes significantly due to the absence of translational invariance and the presence of non-Abelian point-group symmetries. The resulting model exhibits:

- $\mathbb{Z}_2$ **Symmetry (Global Spin Flip):** As in the standard TFIM, the Hamiltonian is invariant under a global spin flip along the x-axis:

$$\sigma_i^x \to -\sigma_i^x, \quad \sigma_i^z \to \sigma_i^z$$

  This discrete symmetry reflects the conservation of parity in the transverse-field term.

- **Time-Reversal Symmetry:** The Hamiltonian remains real and thus invariant under time reversal $\mathcal{T}$:

$$\mathcal{T} : i \to -i, \quad \sigma_i^x, \sigma_i^z \to \sigma_i^x, \sigma_i^z$$

- **Icosahedral Symmetry (I_h):** Instead of translations or reflections, the model now respects the full symmetry group of the icosahedron. This includes:

9

– 60 proper rotations (the icosahedral group I, isomorphic to A_5)

    * 6 five-fold rotation axes passing through opposite vertices, each allowing four nontrivial rotations (72°, 144°, 216°, and 288°).

    These rotations generate a cyclic subgroup $C_5 \subset SO(3)$, consisting of five elements including the identity. Being Abelian, C_5 has five one-dimensional irreducible representations given by

$$\rho_k(r^n) = e^{2\pi i k n/5}, \quad k = 0, 1, 2, 3, 4,$$

    where r is the generator corresponding to a 72° rotation, and $n \in \{0, 1, 2, 3, 4\}$. These representations correspond to the fifth roots of unity and describe how quantum states transform under discrete rotations about a five-fold axis. While this subgroup structure helps organize local symmetries, the full classification of energy eigenstates is governed by the irreducible representations of the full icosahedral group I_h, which contains higher-dimensional non-Abelian representations.

    * 10 three-fold axes passing through opposite face centers (each face being a triangle),

    * 15 two-fold axes passing through the midpoints of opposite edges,

– Inversion symmetry, extending I to the full icosahedral group I_h of order 120,

– No translational symmetry, as the icosahedron is a finite, non-periodic structure.

The eigenstates of the Hamiltonian can thus be classified according to the irreducible representations of I_h, rather than momentum or parity quantum numbers.

- **Absence of Translational and Reflection Symmetries:** The lack of lattice periodicity and mirror planes eliminates discrete translations and standard parity operations found in 1D and higher-dimensional lattices. Instead, symmetry-resolved analysis must be performed in terms of the non-Abelian character table of I_h.

In the standard quantum transverse-field Ising model (TFIM), such as on a one-dimensional chain or higher-dimensional translationally invariant lattices, the symmetry group typically includes a global $\mathbb{Z}_2$ spin-flip symmetry (generated by $\prod_i \sigma_i^x$), along with spatial symmetries such as translations, reflections, and point-group operations, depending on the underlying lattice. These spatial symmetries are often Abelian or contain Abelian subgroups (e.g., cyclic groups for 1D chains), and they play a crucial role in defining momentum sectors, conserved quantities, and the structure of excitations.

By contrast, when the TFIM is defined on the icosahedron—a finite, highly symmetric polyhedron with no translational symmetry—the spatial symmetry group is replaced by the full icosahedral group I_h, a non-Abelian finite group of order 120. This group includes 60 proper rotations forming the icosahedral group I (isomorphic to A_5), along with inversion symmetry. The global $\mathbb{Z}_2$ spin-flip symmetry remains, but the spatial symmetry structure is fundamentally altered: momentum is no longer a good quantum number, and eigenstates are instead organized according to the irreducible representations of I_h. This shift enriches the spectral structure and enables a finer symmetry resolution of both energy levels and entanglement patterns, while also modifying how frustration and degeneracies manifest in the antiferromagnetic case.

As shown in the recent work by Parez and Witczak-Krempa [4], the forward reduction hypothesis (FRH) is always satisfied for reduced density matrices (RDMs) of two spins. Consequently, FRH alone cannot explain the emergence of many-body scars on this lattice. However, for four- and five-spin RDMs, the FRH condition is no longer satisfied for certain eigenstates. In particular, five nearly degenerate scarred eigenstates appear at energy $E = -6$, exhibiting a structure that violates FRH for these larger subsystems. This degeneracy is a direct consequence of the five-fold rotational symmetry of the icosahedron.

These scarred states enable the construction of linear combinations (with complex coefficients) that either minimize or maximize the bipartite entanglement entropy, indicating a highly structured entanglement landscape. A symmetry analysis of these entanglement-minimizing combinations suggests that the scars may be stabilized by nonlocal conserved quantities tied to the icosahedral group, although no local charges commuting with the four- or five-spin RDMs could be identified. This contrasts with systems where many-body scars are explained via locally defined integrals of motion, which typically violate FRH already at the two-spin level.

Further insight comes from analyzing the rank of the RDMs. For generic eigenstates, the four-spin RDM has full rank $2^4 = 16$, while for the five scarred states, the rank is reduced to $16 - 5 = 11$. Similarly,
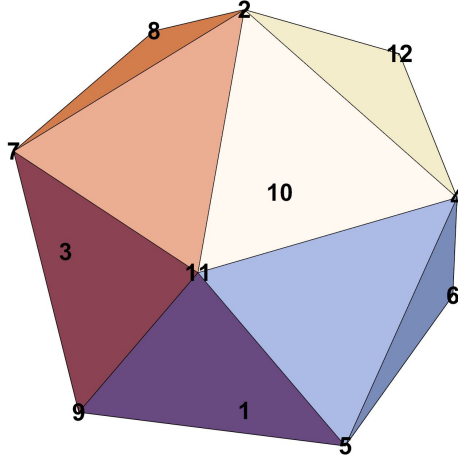
Figure 5: Vertex labeling of the icosahedron used in the TFIM study. Each site interacts with its 5 neighbors via antiferromagnetic Ising couplings.
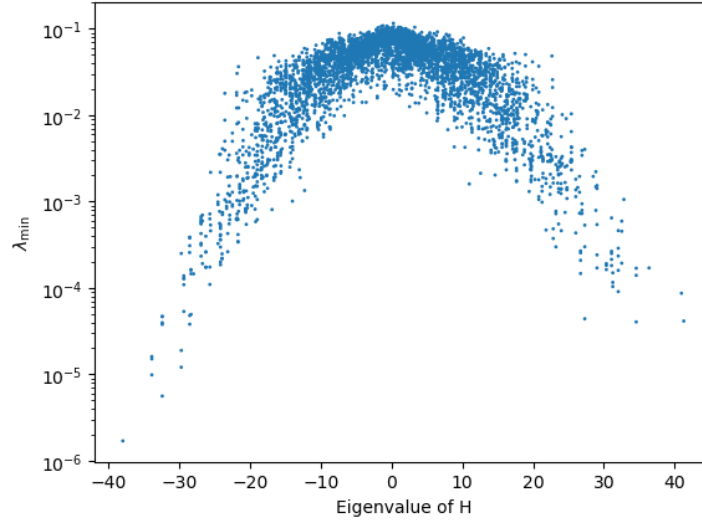

Figure 6: Minimum eigenvalue of the three-spin RDM as a function of the eigenvalue of the Hamiltonian H. FRH is always satisfied; all eigenvalues remain well above machine precision.

the five-spin RDM has full rank $2^5 = 32$ for generic states, and rank 18 for the scarred states, indicating a loss of 14 linearly independent directions. The origin of the number 14 remains an open question, potentially related to hidden symmetries or representation-theoretic properties of the icosahedral group.

add why antiferromagnetic and not ferromagnetic - frustration is only present in the former, i.e. min energy config not reached in a closed loop

For 6 spins rdm, the number of scars increases significantly (441 scarred states for 6 spins rdm) and degeneracy is lifted. for 7+ spins rdm, all states are scarred.

Bibliography

References

[1] S. Sachdev, *Quantum Phase Transitions*, Cambridge University Press (2011).

[2] C. J. Turner, A. A. Michailidis, D. A. Abanin, M. Serbyn, and Z. Papic, "Quantum many-body scars," Nature Physics 14, 745–749 (2018).
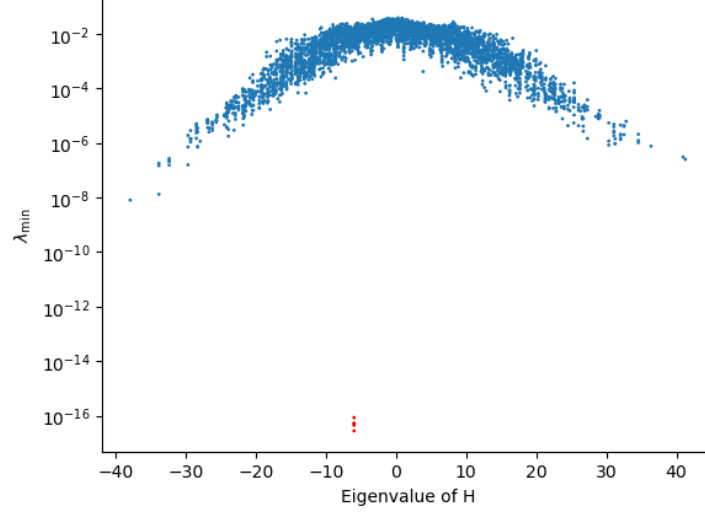
Figure 7: Minimum eigenvalue of the four-spin RDM. Five eigenstates (in red) near $E = -6$ violate FRH with eigenvalues $\lambda_{\min} \sim 10^{-17}$. These correspond to scarred states.
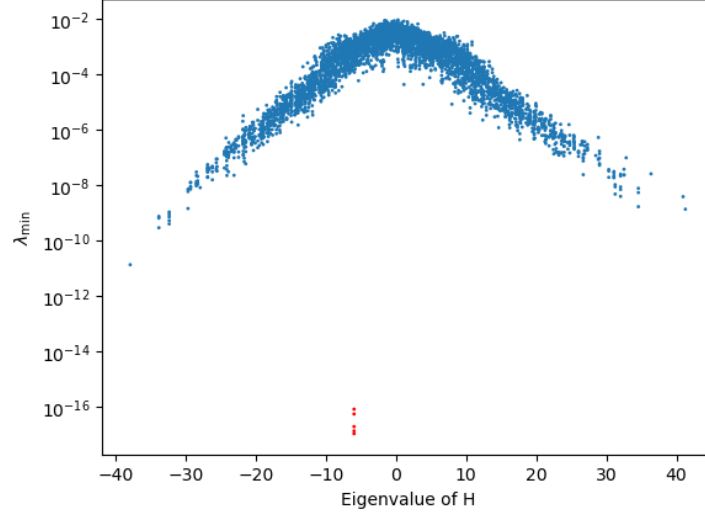

Figure 8: Minimum eigenvalue of the five-spin RDM. The same five scarred states are seen to violate FRH at machine precision.

[3] E. H. Lieb, T. Schultz, and D. Mattis, "Two soluble models of an antiferromagnetic chain," Annals of Physics 16, 407-466 (1961).

[4] G. Parez, W. Witczak-Krempa, "The Fate of Entanglement," arXiv preprint arXiv:2402.06677 (2024).